Atmospheric gamma rays from solar energetic particles and cosmic rays penetrating the magnetosphere

Gerald H. Share and Ronald J. Murphy

E. O. Hulburt Center for Space Research, Naval Research Laboratory, Washington, D.C.

Abstract. We detail observations of gamma rays produced by interactions of cosmic rays and solar-energetic particles on the Earth's atmosphere. The Solar Maximum Mission (SMM*)* spectrometer accumulated the quiescent atmospheric spectrum over its full 9-year lifetime and our analysis revealed 20 resolved line features. We compare this spectrum with one collected on October 20, 1989, when SMM observed gamma rays produced by shock-accelerated protons that impacted the atmosphere in the polar region following an intense solar flare and coronal mass ejection. Observed nuclear-line intensities increased by over a factor of 50 during this event. Because this event was on the horizon and subtended a limited solid angle as viewed from SMM, the local increase was several times higher. We compare the gamma ray line energies, widths, and intensities from the solar event and quiescent atmospheric spectra and discuss their identifications. From this comparison we confirm direct observations that the solar proton spectrum is considerably softer than the spectrum of cosmic rays. Extension of an existing code for calculating solar gamma ray lines will provide information on the spectra of the protons reaching the Earth's atmosphere and thus on their transport through the magnetosphere. Broad spectral features found in the spectra are likely to be caused by a multitude of unresolved lines excited by neutron capture in the instrument, spacecraft, and Earth's atmosphere.

1. Introduction

The Earth's atmosphere is by far the most intense source of gamma radiation observed by satellite-borne spectrometers. Energetic protons in the cosmic radiation and in solar energetic particle events interact with nuclei in the atmosphere to directly excite nuclear states, create reaction products, and produce secondary neutrons. These neutrons also excite nuclear states directly and through products of nuclear reactions. *Letaw et al.* [1989] listed the most intense gamma ray lines from these processes based on earlier compilations by *Ling* [1975], *Ramaty et al.* [1979], and nuclear data tables.

The most comprehensive nuclear-line observations of the quiescent-atmospheric spectrum produced by cosmic ray interactions have been conducted using NASA's HEAO *3* high-resolution [*Mahoney et al.*, 1981; *Willett and Mahoney*, 1992] and SMM moderate-resolution [*Letaw et al.,* 1989] spectrometer experiments. *Willett and Mahoney* [1992] characterized the energies and widths of seven strong lines using the high-resolution capabilities of the germanium detectors and accumulations up to 253 days. In contrast, *Letaw et al.* [1989] identified about 20 lines using atmospheric spectra integrated over a 3.5-year period. In this paper we describe observations of atmospheric gamma rays produced by cosmic ray interactions; these were made by the SMM spectrometer over its full 9-year lifetime.

These quiescent observations are compared with those from a remarkable event discovered by Erich Rieger [*Ryan et al.,* 1999; *Share et al.*, 1999]. This event was observed by the SMM spectrometer at ~1600 UT on October 20, 1989, during an intense solar energetic particle event at the Earth [*Coffey*, 1989; *Boberg et al.*, 1995, and references therein]. The particle event peaked between ~1400 and 1800 UT when the shock from an intense class X13 X-ray flare and high-speed coronal mass ejection, which had occurred ~1300 UT on the previous day, reached Earth. *Boberg et al.*'s [1995] comparison of GOES-7 and NOAA-10 charged-particle observations from October 19 to 27 demonstrate that the particles observed in low-Earth orbit at high geomagnetic latitudes came directly from the shock and not from precipitation of particles in the radiation belts. At the time of the gamma ray event SMM was near Australia, at the most southerly geomagnetic latitude in its orbit. The detector was pointed toward Earth and, with its broad aperture, could view the horizon which was at ~50°S geographic latitude. Calculations with CREME96 [*Tylka et al.*, 1997] indicate that shock-produced particles down to MeV energies should reach the Earth's atmosphere and produce gamma rays detectable by SMM on the southern horizon. Twenty resolved gamma ray line features were identified from this event, the same number that we identified from the quiescent atmosphere. We compare the energies, widths and intensities of the various lines in both these spectra and discuss their origins. In addition to these discrete lines we reveal broad components in both spectra that may be due to a large number of unresolved lines from thermal neutron capture.

2. Observations

The SMM gamma ray spectrometer was in operation in a 28° orbit at ~570 km from February 1980 until November 1989. It was sensitive to gamma radiation from 0.3 to 8.5

Paper number 2000JA002012.
0148-0227/00/2000JA002012$09.00

Report Documentation Page

Form Approved
OMB No. 0704-0188

1. REPORT DATE	2. REPORT TYPE	3. DATES COVERED
2006		**00-00-2006 to 00-00-2006**

4. TITLE AND SUBTITLE	5a. CONTRACT NUMBER
Atmospheric gamma rays from solar energetic particles and cosmic rays penetrating the magnetosphere	5b. GRANT NUMBER
	5c. PROGRAM ELEMENT NUMBER
6. AUTHOR(S)	5d. PROJECT NUMBER
	5e. TASK NUMBER
	5f. WORK UNIT NUMBER
7. PERFORMING ORGANIZATION NAME(S) AND ADDRESS(ES) **Naval Research Laboratory,E. O. Hulburt Center for Space Research,4555 Overlook Avenue, SW,Washington,DC,20375**	8. PERFORMING ORGANIZATION REPORT NUMBER
9. SPONSORING/MONITORING AGENCY NAME(S) AND ADDRESS(ES)	10. SPONSOR/MONITOR'S ACRONYM(S)
	11. SPONSOR/MONITOR'S REPORT NUMBER(S)

12. DISTRIBUTION/AVAILABILITY STATEMENT
Approved for public release; distribution unlimited

13. SUPPLEMENTARY NOTES
JGR, Vol. 106 (Space Physics), No. A1, 77-92, (2001).

14. ABSTRACT

We detail observations of gamma rays produced by interactions of cosmic rays and solar-energetic particles on the Earth?s atmosphere. The Solar Maximum Mission (SMM) spectrometer accumulated the quiescent atmospheric spectrum over its full 9-year lifetime and our analysis revealed 20 resolved line features. We compare this spectrum with one collected on October 20, 1989, when SMM observed gamma rays produced by shockaccelerated protons that impacted the atmosphere in the polar region following an intense solar flare and coronal mass ejection. Observed nuclear-line intensities increased by over a factor of 50 during this event. Because this event was on the horizon and subtended a limited solid angle as viewed from SMM, the local increase was several times higher. We compare the gamma ray line energies, widths, and intensities from the solar event and quiescent atmospheric spectra and discuss their identifications. From this comparison we confirm direct observations that the solar proton spectrum is considerably softer than the spectrum of cosmic rays. Extension of an existing code for calculating solar gamma ray lines will provide information on the spectra of the protons reaching the Earth?s atmosphere and thus on their transport through the magnetosphere. Broad spectral features found in the spectra are likely to be caused by a multitude of unresolved lines excited by neutron capture in the instrument, spacecraft, and Earth?s atmosphere.

15. SUBJECT TERMS

16. SECURITY CLASSIFICATION OF:			17. LIMITATION OF ABSTRACT	18. NUMBER OF PAGES	19a. NAME OF RESPONSIBLE PERSON
a. REPORT **unclassified**	b. ABSTRACT **unclassified**	c. THIS PAGE **unclassified**	**Same as Report (SAR)**	**16**	

MeV and consisted of seven 7.5 × 7.5 cm NaI detectors enclosed in an active CsI anticoincidence shield [*Forrest et al.*, 1980]. The detectors had an ~50 keV full width at half maximum (FWHM) resolution at 1 MeV. The gains of the detectors were actively controlled so precisely that data over the full 9-year mission could be summed together without loss of resolution.

The quiescent spectrum of atmospheric gamma rays was derived from data accumulated in 10.4×10^6 s over a 9-year period at vertical magnetic rigidities <11 GV. We only included data taken at least 10^4 s after the last passage through the radiation belts. In contrast to our earlier study, we included data taken with the instrument's axis pointed up to 72° from the center of the Earth. This spectrum contains instrumental background lines [*Share et al.*, 1988, 1989] in addition to atmospheric radiation. *Letaw et al.* [1989] demonstrated how most of the instrumental radiation can be eliminated by making a time-normalized subtraction of spectra accumulated with the instrument axis pointing away from the Earth. This subtraction was done for each orbit in order to minimize systematic effects. We did not find any evidence for residual radioactive lines in the background- corrected spectrum. However, we did observe residual lines at 1.17 and 1.33 MeV from the onboard ^{60}Co calibration source. The reason for the presence of these residual lines is well understood. The ^{60}Co source was embedded in a plastic scintillation counter that detected the β particle emitted in coincidence with the lines. During normal spectral accumulations, calibration events were rejected when the electrons were detected. However, this rejection was only ~90% effective and was also dependent on orientation of the photomultipliers that viewed the scintillation counter because they were not protected by magnetic shielding. We therefore included lines at these energies in order to fit the spectra.

The background-subtracted spectrum is also moderately distorted because atmospheric radiation leaking into the sky-viewing data is subtracted from the spectrum. This leakage is energy dependent, varying from ~20% of the incident atmospheric flux at 0.3 MeV to ~50% at 5 MeV (J. R. Letaw, unpublished report, 1988). We have corrected the spectrum for this energy dependent effect and plot the resulting count spectrum in Figure 1. The positron annihilation line at 0.511 MeV and its Compton-scattered continuum dominate the spectrum between ~0.3 and 0.55 MeV. A continuum from electron bremsstrahlung, scattered radiation, and various nuclear-line features dominate the spectrum at higher energies.

We also plot the background-corrected count spectrum accumulated from 1550:52 to 1605:04 UT on October 20, 1989, during the peak particle intensity from the interplanetary shock in Figure 1. We used data taken in the 10 min before the event as the background (data were not available just after the event). The overall atmospheric

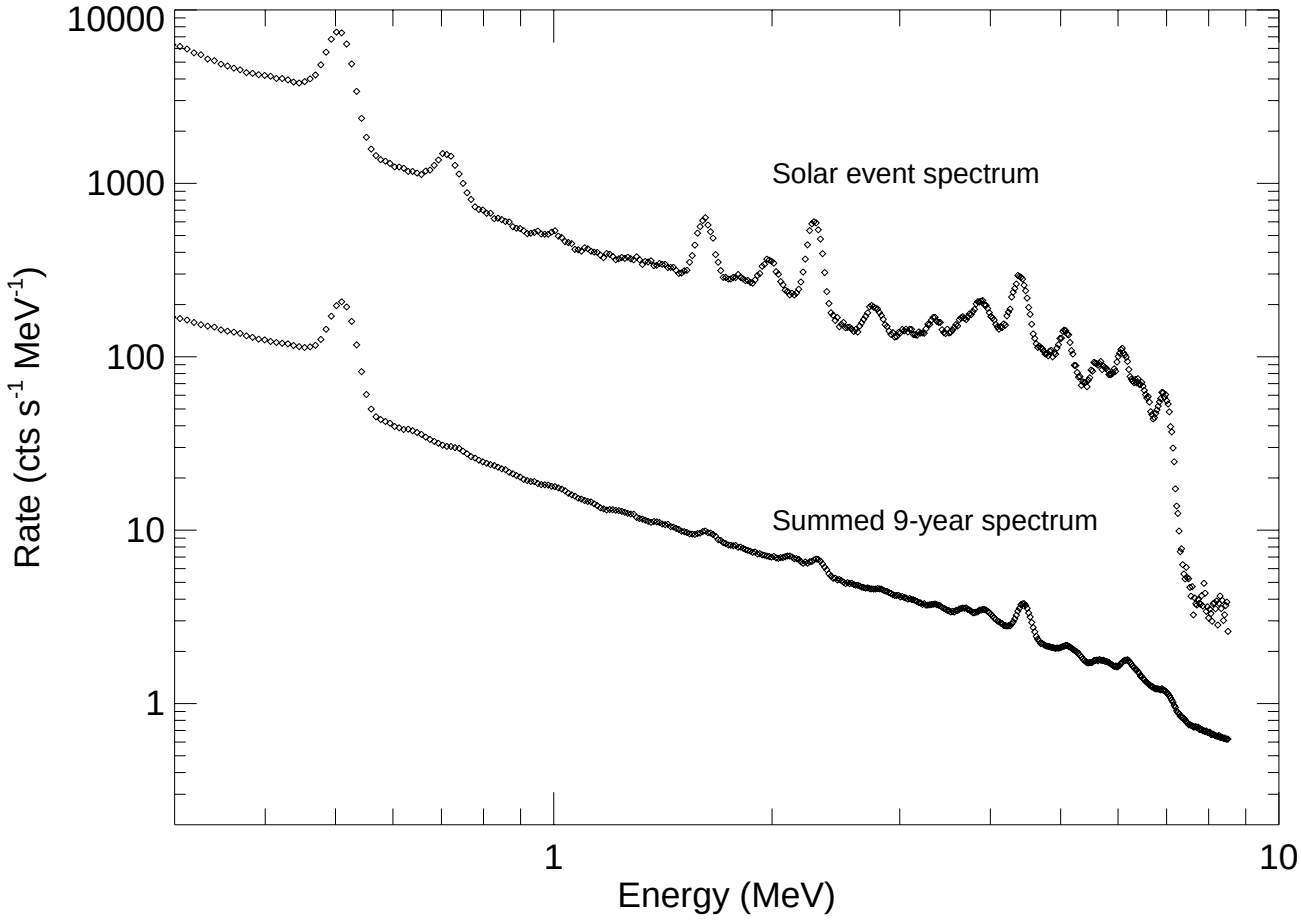

Figure 1. Comparison of the quiescent atmospheric gamma ray spectrum produced by cosmic rays with the spectrum excited by the October 20, 1989, solar energetic particle event (not corrected for instrumental shift).

emission increased ~40-fold during this time interval. The actual increase in the polar region where the particles impacted was several times higher because this region only subtended a small fraction of the instrument's aperture. The observed spectrum is dominated by positron-annihilation and nuclear-line emission. The latter is evidenced by the precipitous fall off in rate above ~7 MeV, where the nuclear contribution ends and contrasts with the relatively stronger continuum from electron bremsstrahlung at these energies observed in the quiescent spectrum. Most of the line features in the quiescent spectrum are strikingly evident in the solar-event spectrum. The lack of a dominant electron-bremsstrahlung continuum in the solar event provides additional evidence that the particles exciting the atmospheric lines do not originate from precipitation from the Earth's radiation belts.

Upon close inspection the features in the solar-event spectrum are slightly shifted (~1%) to lower energy. This shift is purely instrumental and is due to the active gain-control system used by the spectrometer. The gain is controlled using the ^{60}Co calibration source discussed above. In-flight spectra taken in coincidence with electrons detected by plastic scintillation counters during normal accumulations indicated that equal rates were obtained above and below ~1.17 MeV; these spectra are dominated by the calibration sources although chance coincidence of plastic events with the background is possible. Whenever the system measured a photon with energy <1.17 MeV, the gain was increased a step; the opposite occurred when the photon energy was > 1.17 MeV. This system worked so well that we were able to sum data from the full 9-year mission (e.g., the quiescent atmospheric spectrum) without any evidence for line broadening. However, during the intense solar-particle event, the spectrum was harder than the average background thus causing the gain to decrease and the line energies to shift to lower energies.

The annihilation line and its scattered continuum in the solar event do not dominate the other lines as much as they do in the quiescent spectrum. Furthermore the intensity of the Compton-scattered annihilation radiation is lower relative to the line in the solar event. These differences reflect differences between the spectra of cosmic rays and the solar energetic particles. We discuss this in more detail in section 5.2.

3. Spectral Fits

The spectra plotted in Figure 1 are quite complex. There are several line features and resulting instrumental artifacts that are superimposed on a continuum originating from electron bremsstrahlung and scattered radiation. Our basic technique involves constructing incident photon spectra composed of one or two power laws and several line features. These incident spectra were convolved with the instrument response to form predicted-counts spectra that were compared channel by channel with the data [*Letaw et al.*, 1989; *Murphy et al.*, 1990]. This instrument response used energy and width algorithms derived from laboratory calibrations before launch. The response yielded line energies that are ~3 and 13 keV high at 4.4 and 6.1 MeV, respectively, relative to the calibration. We have corrected the energies of the high-energy lines accordingly.

We used an iterative approach to fitting these spectra over the energy range from 0.65 to 8.5 MeV (we discuss fits to the annihilation line in section 3.2 below). Our ultimate goal was to fit simultaneously for all the parameters of the power laws, and the energies, widths, and fluxes of the lines. This procedure is inherently unstable with so many free parameters. In order to accomplish this we initially fixed the line energies and widths at the values determined by *Letaw et al.* [1989] in their study of the atmospheric spectrum. We then incrementally freed these parameters for individual lines, starting from the highest energies and working down in energy. As we stepped down in energy, we included additional Gaussian features when they were necessary to fit the data. Best fitting parameters were determined using a χ^2 minimization algorithm that estimated the uncertainties. However, owing to the complexity of the fit, we found that the variation of χ^2 was sometimes irregular causing errors in this estimation of the uncertainties. We therefore stepped through the energies, widths, and fluxes independently for all the lines and mapped the values of χ^2 to determine both the best fitted parameters and their uncertainties. We used a $\Delta\chi^2$ of 3 to estimate the uncertainties; this provides a 90% statistical confidence that the value is within the uncertainties, assuming that there is only one critical parameter [*Lampton et al.*, 1976]. In order to confirm our fits for the lowest-energy nuclear lines, we performed a separate fit over the energy range from 0.58 to 0.92 MeV.

3.1. Nuclear Lines

The spectra at energies above the annihilation line were fit with 24 Gaussian features superimposed on a continuum that is harder at high energies. The continuum is significantly stronger in the quiescent atmospheric spectrum than in the spectrum produced by the solar shock accelerated particles (see Figure 1).

The quiescent count spectrum from 0.65 to 8.5 MeV is plotted in Figure 2a. The solid line drawn through the points is the best fit. It is formally a poor fit (χ^2/dof [degrees of freedom] = 2.58) but this is largely due to the excellent statistics accumulated in 10.4×10^6 s and limited knowledge of the channel-to-channel properties of the spectral analyzer. The dotted line shows the best fit to the sum of the two power laws that represent the electron continuum radiation. The thin solid line shows the response of the instrument to the 20 individually resolved lines used in the model; the other four Gaussians required to fit the data were very broad and are discussed below.

The count spectrum for the solar event from 0.65 to 8.5 MeV is plotted in Figure 3a. The overall fit, plotted through the data and using summed power laws (electron continuum radiation) and 23 Gaussians, is excellent, χ^2/dof = 1.07 (probability = 18%). Once again the dotted line shows the best fit to the continuum, and the thin solid line represents the response of the instrument to the 20 individually resolved lines used in the model (the three broad Gaussians are discussed below). Note that the energy scale in this figure has not been corrected for the instrumental shift discussed in section 2. We determined this shift by comparing the best fit energy for the resolved ^{14}N deexcitation line with its laboratory value of 1.635 MeV. This comparison yielded a 0.8 % instrumental shift to lower energy.

In Figure 4 we plot the fits to the data that we performed over the limited range from 0.58 to 0.92 MeV in order to

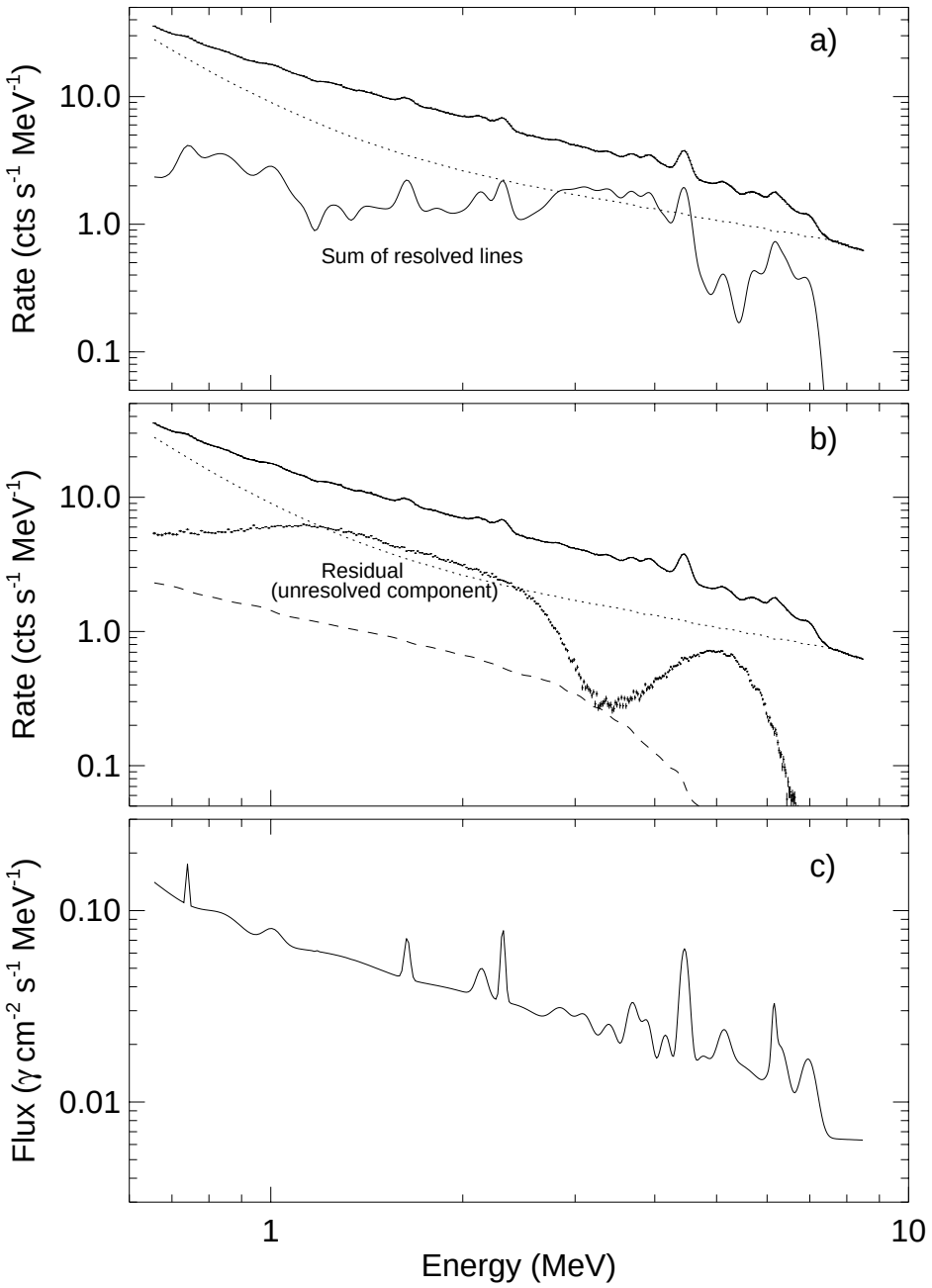

Figure 2. (a) Fit to the quiescent atmospheric gamma ray count spectrum from 0.65 to 8.5 MeV containing electron-bremsstrahlung continuum and 24 nuclear line features. The fit is drawn through the data points; the statistical uncertainties are smaller than the points. The bremsstrahlung component is represented by the sum of two power laws and is shown as the dotted curve. The thin solid line is the instrumental response to the sum of 20 resolved lines. (b) The residual spectrum after subtraction of the 20 resolved nuclear lines and power law continuum. The dashed line shows the shape of the expected Compton scattered continuum produced by the 20 resolved atmospheric lines. For comparison we again plot the full spectrum and power law continuum. (c) The quiescent atmospheric photon spectrum derived from the fit to the SMM data.

improve our line measurements. We fit the quiescent spectrum in Figure 4a with a single power law and three lines. Although only a single significant line is evident in this energy range in the solar-event spectrum plotted in Figure 4b, we again fit the data to a single power law and three lines. We fixed the energies and widths for lines near 0.64 and 0.84 MeV in order to compare limits on their intensities with lines detected in the quiescent spectrum.

We list the fitted energies and widths for 20 resolved lines observed in the quiescent and solar-event spectra in Tables 1 and 2, respectively. The energies of the lines in Table 2 have been corrected for the instrumental shift. The errors in

line energy and width include statistical (from the overall fit) and systematic uncertainties in the fits due to limitations in our knowledge of the energy-to-channel calibration and instrumental line broadening. The measured fluxes in the lines are for a point source assumed to be directly on axis. As the instrument has a broad aperture (~140° FWHM at 0.511 MeV and considerably broader at higher energies), this assumption leads to systematic uncertainties less than 30%. We also list possible line identifications ordered by energy. These identifications are primarily derived from the list published by *Letaw et al.* [1989] with corrections and additions given by *Firestone and Shirley* [1996] Some of

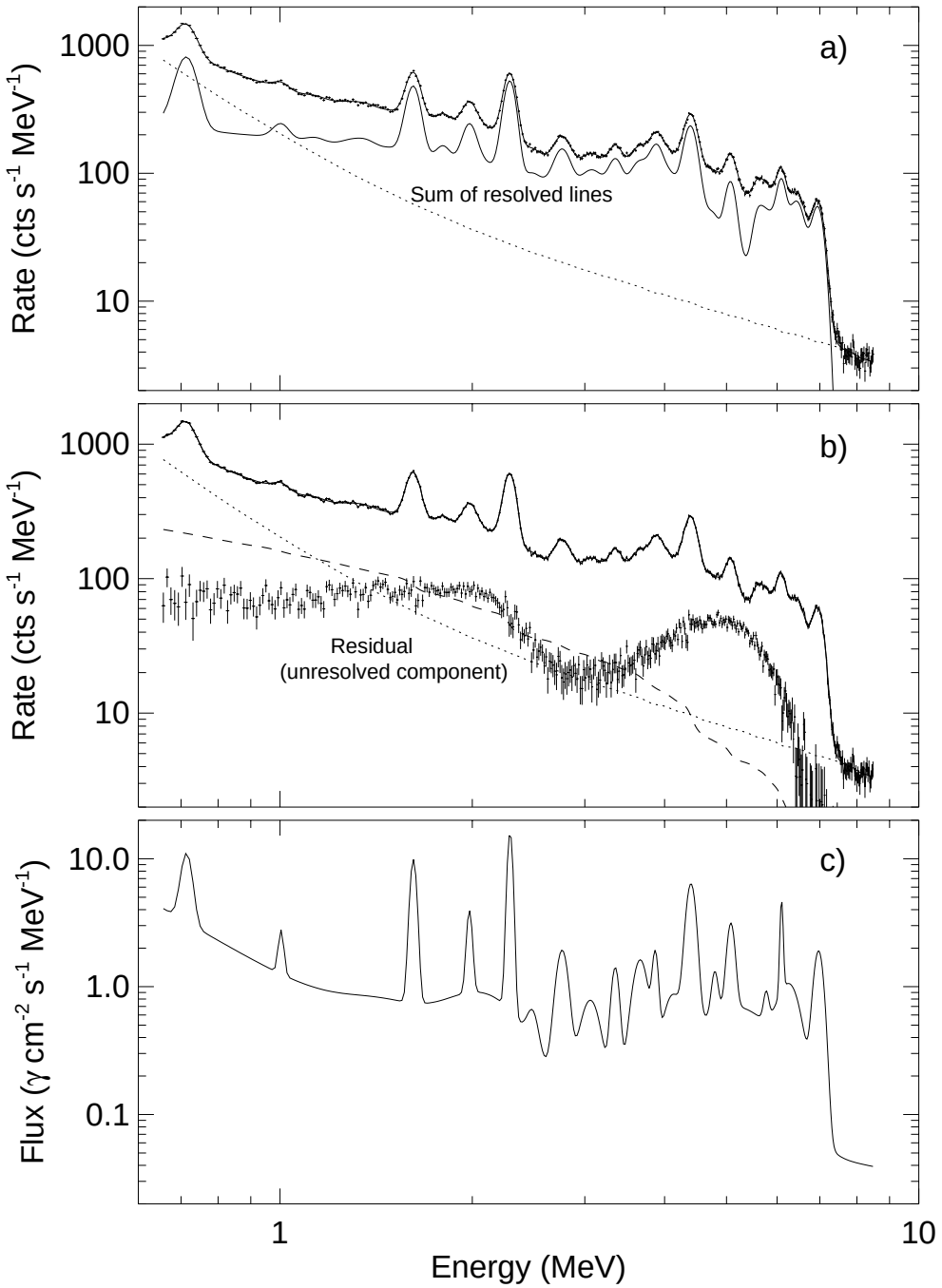

Figure 3. (a) The atmospheric gamma ray count spectrum from 0.65 to 8.5 MeV produced by shock-accelerated particles on October 20, 1989 (not corrected for instrumental shift). The spectrum is fit with a model containing electron-bremsstrahlung continuum and 23 nuclear line features. The bremsstrahlung component is represented by the sum of two power laws and is shown as the dotted curve. The thin solid line is the instrumental response to the sum of 20 resolved lines. (b) The residual spectrum after subtraction of the 20 resolved nuclear lines and power law continuum. The dashed line shows the shape of the expected Compton-scattered continuum produced by the 20 resolved atmospheric lines. For comparison we again plot the full spectrum and power law continuum. (c) The atmospheric photon spectrum from the solar energetic particle event derived from the fit to the SMM data.

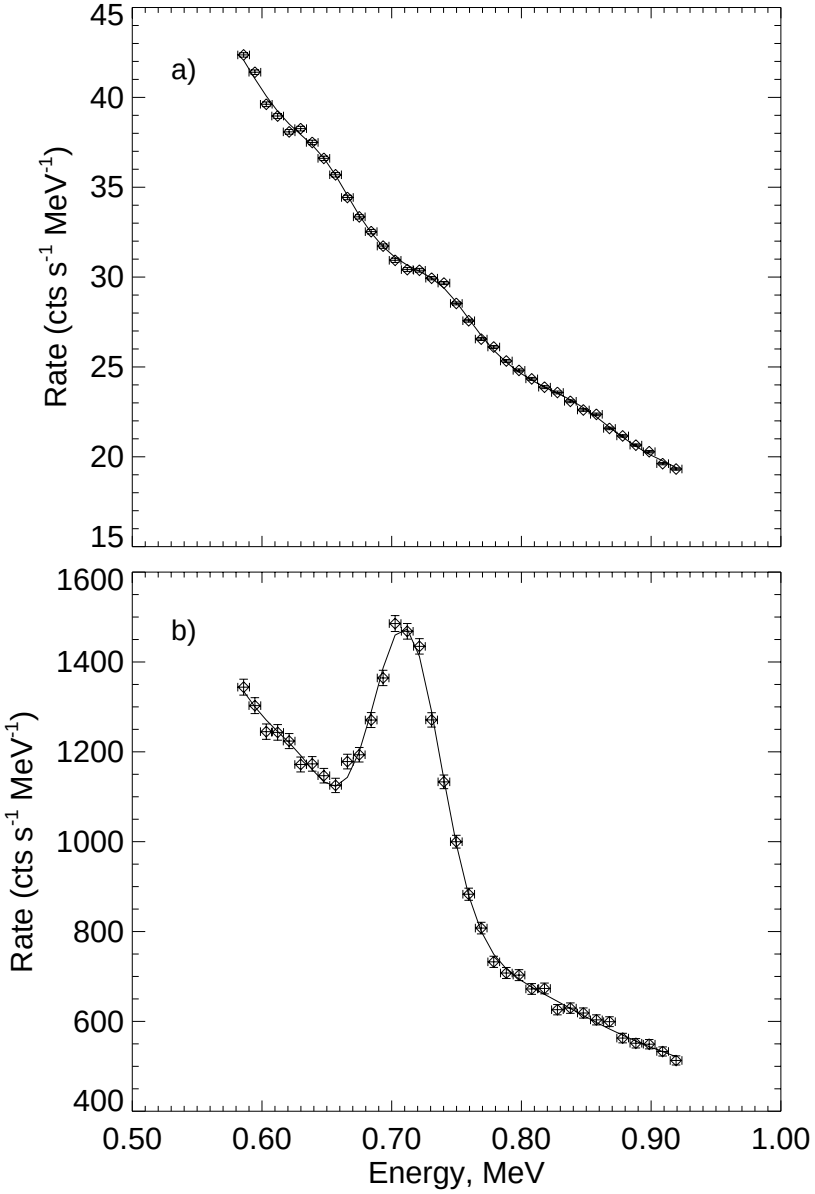

Figure 4. Fits to the atmospheric gamma ray count spectra over the limited range from 0.58 to 0.92 MeV. The model includes a power law continuum and three Gaussian line features. (a) Quiescent spectrum from cosmic ray interactions. (b) Spectrum from interaction of solar energetic particles (not corrected for instrumental shift).

these lines result from direct excitation of ^{14}N and ^{16}O by neutrons and protons, for example, the 1.635 MeV line from ^{14}N. Others result from spallation products of the target ^{14}N and ^{16}O nuclei, for example, the 4.44 MeV line from ^{11}B and ^{12}C. We list only the most intense lines in the range of the spectrometer. Some of these lines come from excited states with energies above 10 MeV.

There are many weaker lines that are not included in Tables 1 and 2 that are not resolved individually and form broad spectral features. In order to improve our fits to the data, we found it necessary to include broad unresolved components to account for these features. As a first approximation, we found that four Gaussians were required to fit the quiescent spectrum. The center energies (widths, FWHM) of these Gaussians are, 1.25 (0.70), 1.75 (0.82), 2.52 (0.70), and 5.3 (1.8) MeV. Three broad Gaussians with energies (widths) of 1.44 (0.60), 2.12 (0.60), and 5.24 (1.70) MeV were also needed to adequately fit the solar-event spectrum. We can reveal the shape of these unresolved line continua by subtracting the best fitting electron continuum radiation (dotted line) and the sum of resolved lines (thin solid line) from the data plotted in Figures 2a and 3a. The residual spectra obtained from these subtractions are plotted in Figures 2b and 3b, along with the original data, the full fit, and the power-law continuum for comparison. Broad Gaussian-like features are clearly present near 5 MeV in both residual spectra. The residuals also contain extended unresolved components below 3 MeV. We discuss a possible thermal neutron capture origin for these broad features in section 5.4. There is no evidence for strong individually resolved lines in the residuals. This suggests that our fits have successfully identified most of these lines. However, there is weak evidence for some structure that may be due to blended weak lines in the quiescent residual above 5 MeV.

TABLE 1 RESOLVED ATMOSPHERIC LINES FROM COSMIC-RAY INTERACTIONS

Energy, keV	Width(FWHM), keV	Flux, $10^{-4}\gamma/cm^2$-s	Identification (keV)
513.0 ± 3.0	12.9 ± 8.0	343.0 ± 5.0	e^+-e^- annihilation line
645.0 ± 10.0	?	6.0 ± 2.0	?, ^{14}C (613, 634)
735.0 ± 5.0	9.4 ± 7.0	6.0 ± 2.0	^{10}B (718); ^{14}N (728)
842.0 ± 5.0	?	3.0 ± 2.0	?, ^{14}C (808)
1008.0 ± 10.0	75.2 ± 35.3	11.0 ± 4.0	^{10}B (1022)
1635.0 ± 3.0	≤ 30.0	11.0 ± 1.0	^{15}O (1617); ^{14}N (1635)
2145.0 ± 15.0	105.7 ± 58.7	15.0 ± 5.0	^{11}B (2124); ^{10}B (2154)
2311.0 ± 3.0	≤ 30.0	21.0 ± 3.0	^{15}N (2297); ^{11}B (2298); ^{14}N (2313); ^{13}N (2365)
2860.0 ± 50.0	≤ 460.0	35.0 ± 35.0	^{16}O (2741); ^{14}N (2793);^{10}B (2868)
3110.0 ± 30.0	282.0 ± 164.5	50.0 ± 30.0	^{14}N (3073), ^{13}C (3089)
3390.0 ± 20.0	329.0 ± 141.0	45.0 ± 20.0	^{14}N (3378, 3384), ^{16}O (3439)
3690.0 ± 20.0	≤ 350.0	50.0 ± 30.0	^{14}N (3674), ^{13}C (3684)
3880.0 ± 50.0	≤ 230	35.0 ± 15.0	^{16}O (3839), ^{13}C (3853); ^{14}N (3890)
4140.0 ± 25.0	258.5 ± 94.0	31.0 ± 4.0	^{16}O (4179)
4449.0 ± 4.0	157.4 ± 14.0	88.0 ± 5.0	^{14}N (4402), ^{12}C (4439); ^{11}B (4444)
4700.0 ± 50.0	305.5 ± 94.0	9.0 ± 2.0	^{11}B (4666, 4739); ^{11}C (4803)
5124.0 ± 10.0	293.8 ± 35.6	24.0 ± 6.0	^{16}O (4966), ^{14}N (5105); ^{15}O (5180)
6139.0 ± 6.0	96.3 ± 21.0	16.0 ± 3.0	^{16}O (6129); ^{15}O (6175); ^{14}N (6202)
6280.0 ± 30.0	411.2 ± 58.7	44.0 ± 4.0	^{14}N (6202, 6445); ^{15}N (6322); ^{11}C (6337)
6950.0 ± 10.0	444.1 ± 12.9	47.0 ± 4.0	^{16}O (6917, 7115); ^{14}C (7010); ^{14}N (7027)

We have investigated whether Compton-scattered radiation from the resolved lines contributes significantly to the residual features in both spectra. The shape of the Compton- scattered radiation is dependent on the geometry of source. To first approximation we have assumed that the Compton spectrum is flat below the line energy and have normalized its total yield to the measured line flux for a given depth in nitrogen. (The actual Compton spectrum is probably somewhat steeper below ~1 MeV). We then summed up the Compton contributions from all the lines and displayed the results as the dashed curves in Figures 2b and 3b. The shapes are vastly different from the residuals and thus cannot be a large fraction of the total emission. Fits to the spectra with these Compton contributions suggest that the lines originate at rather shallow depths in the atmosphere (significantly less than the depths for the annihilation line). In Figures 2c and 3c we plot our best estimates of the photon spectra from the quiescent and solar

TABLE 2 RESOLVED ATMOSPHERIC LINES FROM SOLAR-PARTICLE EVENT

Energy, keV	Width(FWHM), keV	Flux, $10^{-2}\gamma/cm^2$-s	Identification (keV)
512.1 ± 3.0	17.6 ± 5.8	129.0 ± 1.0	e^+-e^- annihilation line
719.7 ± 3.0	30.5 ± 8.2	27.4 ± 1.0	^{10}B (718); ^{14}N (728)
1012.0 ± 6.0	≤ 46.0	4.0 ± 0.5	^{10}B (1022)
1629.9 ± 3.0	32.0 ± 7.0	41.0 ± 2.0	^{15}O (1617); ^{14}N (1635)
1994.8 ± 5.0	70.5 ± 47.0	14.0 ± 2.0	^{11}C (2000); ^{15}N (1997)
2298.2 ± 15.1	43.0 ± 10.0	79.0 ± 6.0	^{15}N (2297); ^{11}B (2298); ^{14}N (2313)
2499.8 ± 40.3	≤ 630.0	4.0 ± 4.0	^{14}N (2414, 2497, 2518); unresolved lines
2787.1 ± 5.0	124.5 ± 21.7	24.0 ± 3.0	^{16}O (2741); ^{14}N (2793); ^{10}B (2868)
3087.5 ± 15.1	258.5 ± 70.5	16.0 ± 2.0	^{14}N (3073), ^{13}C (3089)
3376.8 ± 13.1	117.5 ± 47.0	15.0 ± 3.0	^{14}N (3378, 3384),^{16}O (3439)
3679.2 ± 30.2	223.2 ± 94.0	31.0 ± 6.0	^{14}N (3674), ^{13}C (3684)
3890.9 ± 20.2	≤ 270.0	14.0 ± 6.0	^{16}O (3839),^{13}C (3853); ^{14}N (3890)
4183.2 ± 151.2	≤ 600.0	15.0 ± 9.0	^{16}O (4179)
4435.0 ± 5.0	159.8 ± 14.0	100.0 ± 8.0	^{14}N (4402), ^{12}C (4439); ^{11}B (4444)
4835.0 ± 30.2	117.5 ± 70.5	10.0 ± 2.0	^{11}C (4803); ^{14}N (4914)
5115.0 ± 10.1	152.8 ± 23.5	40.0 ± 4.0	^{16}O (4966), ^{14}N (5105); ^{15}O (5180)
5800.0 ± 45.4	≤ 280.0	4.0 ± 3.0	^{14}N (5833); ^{11}B (5851)
6133.0 ± 8.0	63.4 ± 46.3	28.0 ± 4.0	^{16}O (6129); ^{15}O (6175); ^{14}N (6202)
6320.0 ± 26.2	587.5 ± 117.5	44.0 ± 10.0	^{14}N (6202, 6445); ^{15}N (6322); ^{11}C (6337)
7010.0 ± 10.0	274.9 ± 20.6	53.0 ± 2.0	^{16}O (6917, 7115); ^{14}N (7027)

event excited atmospheres.

3.2. Annihilation Line

We separately fit the spectra near the annihilation line. The spectra were fit from 0.35 to 0.62 MeV with an incident photon model containing a single power law, the annihilation line, and a continuum representing its Compton-scattered continuum. We do not expect a positronium continuum from the triplet state because of the high atmospheric density. The spectra and best fitting models are shown in Figure 5 from the quiescent (Figure 5a) and the solar event (Figure 5b) excited atmospheres. The fitted line parameters are also given in Tables 1 and 2.

4. Comparison with Earlier Observations of the Quiescent Atmosphere

We compare the present observations of the quiescent atmospheric spectrum produced by cosmic rays with those published previously. As this work is an extension of the *Letaw et al.* [1989] study, we expect similar results with improved statistics. This is indeed the case. Our current study reveals additional resolved line features near 0.64, 0.84, 1.01, and 4.7 MeV that were not found in the spectra accumulated over only the first 3.5 years of the mission. We note that in a subsequent unpublished study [*Letaw*, 1988], where spectra were integrated over 7.2 x 10^6 s, lines at ~0.82 and 1.005 MeV did begin to appear. Letaw identified lines at ~5.6 and 5.8 MeV which we do not list specifically in Table 1; these features were difficult to distinguish from the first escape peak and Compton edge from the 6.13 MeV line.

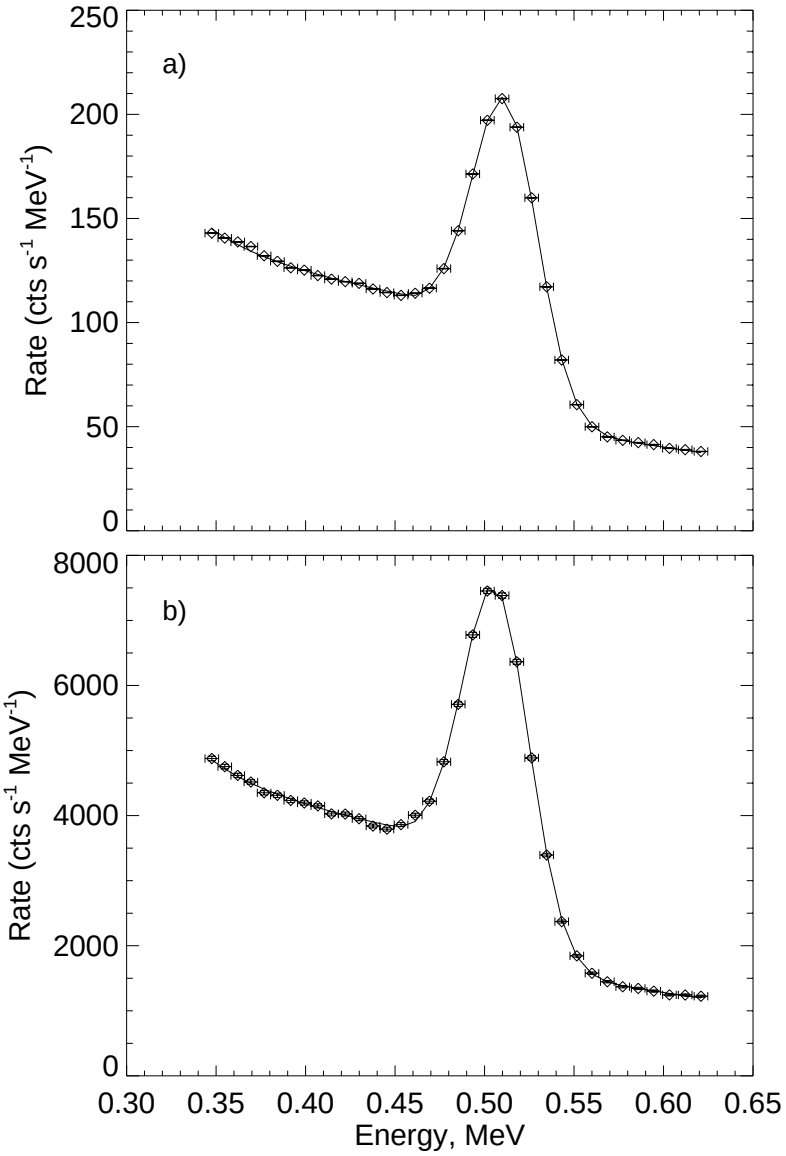

Figure 5. Fits to the atmospheric gamma ray count spectra over the limited range from 0.35 to 0.62 MeV. The model includes a power law continuum, annihilation line and Compton-scattered radiation. (a) Quiescent spectrum from cosmic ray interactions. (b) Spectrum from interaction of solar energetic particles (not corrected for instrumental shift).

TABLE 3 COMPARISON OF *SMM* AND *HEAO-3* LINE OBSERVATIONS

Lab	Energy, keV		Width (FWHM), keV		Flux, $10^{-4}\gamma/cm^2$-s-sr	
	SMM	*HEAO-3*	*SMM*	*HEAO-3*	*SMM*	*HEAO-3*
511	513.0 ± 3.0	511.07 ± 0.1	12.9 ± 8.0	2.29 ± 0.3	85.6 ± 1.3	110.6 ± 2.2
1635	1635.0 ± 3.0	1634.8 ± 1.4	≤ 30.0	20.2 ± 5.7	2.8 ± 0.3	3.4 ± 0.8
2313	2311.0 ± 3.0	2309.4 ± 1.9	≤ 30.0	24.0 ± 5.4	5.3 ± 0.8	5.4 ± 0.8
3684	3690.0 ± 20.0	3673.0 ± 4.7	≤ 350.0	70 ± 15	12.5 ± 7.5	4.0 ± 1.0
4.439, 4444	4449.0 ± 4.0	4428.5 ± 7.5	157.4 ± 14.0	135 ± 12	22.0 ± 1.3	19.6 ± 2.1
5105, 5180	5124.0 ± 10.0	5090.2 ± 10.4	253.4 ± 9.2	95 ± 26	6.0 ± 1.5	3.4 ± 1.2
6129, 6170	6139.0 ± 6.0	6137.2 ± 10.2	96.3 ± 21.0	98 ± 27	4.0 ± 0.8	5.4 ± 1.5

4.1. Comparison with high-resolution spectra

We have compared our fits to lines in the quiescent atmospheric spectrum with those obtained by *Mahoney et al.* [1981] and by *Willett and Mahoney* [1992] using the high-resolution germanium spectrometer onboard HEAO 3. This instrument had an ~3 keV FWHM resolution at 1 MeV at the start of the mission, but this degraded to ~6 keV after 100 days. In Table 3 we list the energies, widths, and intensities of those lines measured by both HEAO 3 and SMM. The SMM line intensities were derived by dividing the values in Table 1 by the solid angle subtended by the Earth as viewed from an altitude of 450 km. The line intensities observed by SMM and HEAO 3 are in remarkably good agreement for those features with comparable widths. The SMM features at 3.68 and 5.1 MeV are significantly broader than those observed by HEAO and may contain additional unresolved lines to weak to be observed by HEAO 3; this resulted in higher fluxes measured by SMM.

The SMM and HEAO 3 line energies are also in good agreement. The HEAO 3 4.4 MeV line measurements falls slightly below the laboratory values [*Willett and Mahoney*, 1992]. The ~6.1 MeV line feature is likely to be a composite of more than one line and thus the measured energy will depend on their relative intensities. The SMM line widths in Table 3 are in general larger and more uncertain than those measured by HEAO 3. SMM recorded an annihilation line width of 12.9 ± 8.0 keV, FWHM, ~1 σ higher than the 2.3 keV recorded by HEAO 3. The SMM measurement of atmospheric line width is strongly dependent on knowledge of the instrumental broadening. We have included an estimate of this uncertainty in the errors listed. At 0.511 MeV the instrumental width is ~40 keV. An error in the knowledge of this width of ~1 to 2 keV is sufficient to account for the disagreement with HEAO 3.

The direct deexcitation lines from ^{14}N should dominate the features at 1.6 and 2.3 MeV. The HEAO widths measured for these lines are consistent with a Doppler broadening of ~1 % [*Murphy*, 1985]. The SMM limits on line widths at these energies are consistent with those measured by HEAO 3. The feature at ~3.684 MeV is identified with two nearby lines in the Table 1, from ^{13}C and from ^{14}N. The HEAO 3 width measurement suggests increased Doppler broadening, ~1.9%. This may be due to additional recoil in the higher energy ^{14}N (n, d) ^{13}C reaction. The width of the line measured by SMM is highly uncertain. The SMM width for the 4.44 MeV feature is only ~1 σ higher than the HEAO 3 measurement. This feature is identified with two nearby lines from spallation products of the ^{14}N target, ^{11}B at 4.444 MeV, and ^{12}C at 4.438 MeV. Because this 6 keV difference in energy is small relative to the observed Doppler broadening of ~3%, it is likely that the increased broadening comes from larger recoil in the higher energy ^{14}N (n, t) ^{12}C and ^{14}N (n, α) ^{11}B spallation reactions. The feature near 5.1 MeV is likely to be a composite; this may account for the large width measured by SMM, although the feature did not appear to be significantly broadened in the HEAO data.

The width of the feature near 6.1 MeV measured by SMM is in excellent agreement with that measured by HEAO 3. The width of the feature, ~1.6%, is larger than that expected for Doppler broadening from directly excited ^{16}O. This suggests that there may be contributions from ^{14}N and ^{15}O at higher energies. The presence of one or both of these lines may also have shifted the energy of the feature above the 6.129 MeV expected from ^{16}O.

In summary we find that the SMM line energies, widths and fluxes are in good agreement with those made by the high-resolution HEAO 3 instrument for the quiescent atmospheric spectrum produced by cosmic ray collisions.

5. Comparison of the Solar Event and Quiescent Atmospheric Spectra

Atmospheric ^{14}N and ^{16}O are the primary targets for particle interactions in the upper atmosphere. Owing to the 28° inclination of the SMM orbit, the minimum magnetic-rigidity cutoff is ~2 GV. Cosmic ray protons at these energies primarily produce spallation products and neutrons [*Ling*, 1975] rather than directly excite nuclei. This is true because the cross sections for direct excitation peak in the vicinity of 10 MeV, considerably below the geomagnetic cutoff for the primary protons, while spallation-reaction cross sections continue to higher energies. It is the secondary neutrons with energies between ~5 and 100 MeV that are responsible for most of the atmospheric gamma rays, through both direct excitation and spallation.

In contrast, protons from the interplanetary shock on October 20, 1989 are primarily responsible for the gamma rays observed by SMM, through both direct excitation and spallation of atmospheric ^{14}N and ^{16}O. This is the case because SMM was viewing regions of the Earth's atmosphere that could be reached by protons of all energies due to the disturbed geomagnetic conditions. Although we expect that most of the lines observed in the quiescent spectrum would also be detected in the solar-event spectrum,

TABLE 4 COMPARISON OF *SMM* ATMOSPHERIC LINE OBSERVATIONS

Energy, keV		Width (FWHM), keV		Quiescent/Solar
Quiescent	Solar Event	Quiescent	Solar Event	Flux Ratio
513.0 ± 3.0	512.1 ± 3.0	12.9 ± 8.0	17.6 ± 5.8	9.9 ± 1.0
645.0 ± 10.0				16.0 ± 13.0
735.0 ± 5.0	719.7 ± 3.0	9.4 ± 7.0	30.5 ± 8.2	0.8 ± 0.3
842.0 ± 5.0				54.5 ± 275.1
1008.0 ± 10.0	1012.0 ± 6.0	75.2 ± 35.3	≤ 46.0	10.3 ± 4.1
1635.0 ± 3.0	1629.9 ± 3.0	≤ 30.0	32.0 ± 7.0	1.0 ± 0.2
2311.0 ± 3.0	2298.2 ± 15.1	≤ 30.0	43.0 ± 10.0	1.0 ± 0.2
2860.0 ± 50.0	2787.1 ± 5.0	≤ 460.0	124.5 ± 21.7	5.4 ± 5.5
3110.0 ± 30.0	3087.5 ± 15.1	282.0 ± 164.5	258.5 ± 70.5	11.6 ± 7.2
3390.0 ± 20.0	3376.8 ± 13.1	329.0 ± 141.0	117.5 ± 47.0	11.2 ± 5.6
3690.0 ± 20.0	3679.2 ± 30.2	≤ 350.0	223.2 ± 94.0	6.0 ± 3.8
3880.0 ± 50.0	3890.9 ± 20.2	≤ 230.0	≤ 270.0	9.3 ± 5.7
4140.0 ± 25.0	4183.2 ± 151.2	258.5 ± 94.0	≤ 600.0	7.7 ± 4.8
4449.0 ± 4.0	4435.0 ± 5.0	157.4 ± 14.0	159.8 ± 14.0	3.3 ± 0.5
4700.0 ± 50.0	4835.0 ± 30.2	305.5 ± 94.0	117.5 ± 70.5	3.4 ± 1.1
5124.0 ± 10.0	5115.0 ± 10.1	293.8 ± 35.6	152.8 ± 23.5	2.2 ± 0.6
6139.0 ± 6.0	6133.0 ± 8.0	96.3 ± 21.0	63.4 ± 46.3	2.1 ± 0.5
6280.0 ± 30.0	6320.0 ± 26.2	411.2 ± 58.7	587.5 ± 117.5	3.7 ± 1.0
6950.0 ± 10.0	7010.0 ± 10.0	444.1 ± 12.9	274.9 ± 20.6	3.3 ± 0.5

there should be differences because the quiescent neutron spectrum is significantly harder than the proton spectrum from the shock on October 20, 1989. The index of the power law fit to the atmospheric neutron spectrum is harder than –1.5 [*Lockwood et al.*, 1979], while the index for the shock protons observed by *GOES* is softer than –2 in the 10–100 MeV range.

In sections 5.2 and 5.3 we compare details of the gamma ray lines from cosmic ray and solar-particle irradiation of the atmosphere listed in Tables 1 and 2. In order to make this comparison easier, we list the fitted energies and widths of the line features in Table 4. In the last column we list the ratio of the line fluxes in the quiescent and solar-particle produced spectra, normalized to the ratio observed in the ^{14}N deexcitation line at 1.635 MeV. We expect that flux ratios close to unity indicate that the gamma ray line originated from a low-energy nuclear state created by a direct excitation. A ratio significantly larger than unity suggests a strong contribution from spallation products due to the harder quiescent particle spectrum.

5.1. Electron Continuum Radiation

The electron bremsstrahlung (and scattered) continuum originates from electron showers that follow decay of π-mesons and β-unstable nuclei. Proton energies in excess of a few hundred MeV are required to produce the pions; therefore we would expect that the bremsstrahlung continuum would be significantly stronger, relative to nuclear lines, from the cosmic rays than from the solar shock-accelerated particles. We have fitted the bremsstrahlung continuum in both the quiescent and solar-event spectra as the sum of two power laws above 0.65 MeV. The parameters derived for the power laws are listed in Table 5. The spectral indices derived for the quiescent continuum are harder than those derived for the solar event, consistent with the harder spectra of the incident cosmic rays. While the low-energy power laws are dominated by the spectra from showering electrons, the flat high-energy power laws in both spectra suggest an origin from a harder electron component such as from π–μ–e decay. The bremsstrahlung intensity during the solar particle event is about a factor of 25 higher than that in the 9-year averaged atmospheric spectrum. In contrast the 1.635 MeV nuclear line from ^{14}N is ~400 times higher in the solar-event spectrum. This once again suggests a stronger contribution of shock accelerated protons in the 1–20 MeV energy range during the solar event.

5.2. Annihilation Line and Continuum

The energies and widths of the quiescent and solar event annihilation lines are consistent with one another. The line and its continuum have their origins in the annihilation of

TABLE 5 COMPARISON OF ATMOSPHERIC BREMSSTRAHLUNG OBSERVATIONS

	Amplitude $10^{-2}\gamma cm^{-2}s^{-1}$ @ 1 MeV		Exponent	
	Quiescent	Solar Event	Quiescent	Solar Event
Low-Energy Power Law	4.0 ± 0.3	95.8 ± 11.8	-2.78 ± 0.03	-3.19 ± 0.19
High-Energy Power Law	0.74 ± 0.03	27.8 ± 12.0	-0.08 ± 0.02	-0.93 ± 0.19

positrons produced both from the decay of β^+-unstable nuclei and from electromagnetic showers from decay of pions produced by high-energy interactions. Owing to the hardness of the cosmic ray spectrum, we expect that the latter source would dominate the quiescent spectrum; the strong bremsstrahlung continuum in the 9-year quiescent spectrum, which has the same shower origin, is consistent with this premise. The quiescent 0.511-MeV line is 10 times more intense, relative to the nuclear lines, than the line produced by the solar energetic particle event. This difference again arises from the harder cosmic ray spectrum.

The width of the 0.511 keV line measured by the HEAO 3 [*Mahoney et al.,* 1981] high-resolution spectrometer is only ~2 keV (FWHM). Widths this narrow are impossible to measure with NaI detectors, such as those on SMM, that have instrumental widths of ~40 keV at this energy. As discussed in section 4.1, a 1–2 keV underestimate in the instrumental width would produce the 511-keV line widths ≥10 keV that SMM observed in both spectra.

The relative flux in the Compton-scattered annihilation radiation below the 511-keV line provides an estimate of the depth in the atmosphere where the positrons annihilate. The fluxes of scattered-annihilation radiation above 0.3 MeV in the quiescent and solar-event spectra are 0.047 ± 0.001 and 1.62 ± 0.03 γ cm^{-2} s^{-1}, respectively. These scattered fluxes are 1.37 ± .03 and 1.26 ± .03 times those in the 511 keV line listed in Tables 1 and 2, respectively. These ratios are also dependent on the location of the gamma ray source on the Earth. Since the solar particle event occurred on the Earth's limb, the atmospheric column depth observed is greater than the true perpendicular depth. The quiescent gamma rays are distributed more uniformly over the Earth, although there is expected to be some limb brightening as well [*Mahoney et al.*, 1981]. These comparisons indicate that the mean Compton-scattering depth of the annihilation line is greater for the cosmic ray produced spectrum than it is for the solar-energetic particle produced spectrum. This is consistent with the more penetrating nature of the cosmic rays. *Letaw et al.* [1989] estimated that annihilation takes place at an effective atmospheric depth of ~21 g cm^{-2} for the cosmic radiation based on measurement of the scattered annihilation radiation.

5.3. Resolved Nuclear Lines

As explained by *Ling* [1995], the lines in the quiescent atmospheric spectrum generated by galactic cosmic rays are predominately the result of interactions by secondary neutrons. In contrast the lines excited in the atmospheric spectrum during the solar event are primarily from proton interactions. We would expect to see basic similarities between the quiescent and solar event line spectra, but there should also be differences. For example, one would expect the quiescent atmospheric spectrum to contain stronger ^{14}C deexcitation lines due to the ^{14}N(n, p)^{14}C reaction. Lines at 0.495, 0.613, 0.634, 0.808, 1.248, 6.092, 6.726, and 7.010 MeV are expected from ^{14}C. The line at 0.495 MeV is too close to the annihilation feature to be detectable. The quiescent atmospheric spectrum does reveal features near ~0.65 and ~0.84 MeV, not observed in the spectrum produced by solar energetic particles, that may in part be due to ^{14}C. A highly broadened feature near 1.23 MeV may also be in part due to ^{14}C.

Below we discuss the resolved line features based on the information in Tables 2–4. The line energies, widths, and relative fluxes provide a basis for identifying the contributing isotopes. The quiescent/solar event flux ratio (normalized to the ^{14}N deexcitation line at 1.635 MeV) is also a diagnostic. We expect features that are individually resolved direct excitation lines to have flux ratios close to unity and those having contributions from high-energy spallation reactions to have higher ratios. For example, we find flux ratios consistent with unity for the ~0.73 and 2.313 MeV lines, thus confirming that directly excited ^{14}N is the primary source of these features. In cases where these lines originate from excited states above 10 MeV, we also expect that the flux ratio may exceed unity due to the harder cosmic ray spectrum.

1. The ~0.64 MeV feature is detected at about the 3 σ level in the quiescent spectrum and not observed at a significant level in the solar-event spectrum (we did fit the line in order to get a limit on its intensity). It may be due to deexcitation of ^{14}C (0.613 and 0.634 MeV), produced by the (n, p) reaction on ^{14}N, although the energy appears to be high. It is difficult to obtain a reliable measurement of the line width in this region of the spectrum where the continuum dominates. The quiescent/solar line flux ratio is uncertain.

2. The ~0.72 MeV line is clearly revealed in both the quiescent and solar-event spectra with energies close to deexcitation of ^{14}N (0.728 MeV). The width of the quiescent line is consistent with the expected ~1% (FWHM), but the solar-event line appears to be broadened to ~3%. The intensity ratio is close to unity, suggesting that ^{14}N is the primary contributor. However, the 0.718 MeV line from ^{10}B may also contribute (see discussion of the ~1.01 MeV line). The 0.728 MeV line comes from the 5.834 MeV excited state and has a branching ratio ~3.7 times larger than deexcitation to the ground state. This is consistent with the low intensity found for the 5.833 MeV line in the solar spectrum and our inability to detect it in the atmospheric spectrum. Both of these lines were too weak to be detected by the HEAO 3 spectrometer.

3. The ~0.84 MeV feature is only weakly detectable in the quiescent atmospheric spectrum, and its width is uncertain. The ^{14}C (0.808 MeV) line lies 30 keV below the fitted energy. If the feature is due to this line, then a more intense line should be observed at 6.092 MeV. However, this line could not be resolved from the 6.129 MeV line from ^{16}O. HEAO 3 did not detect any line features near 0.8 MeV. The quiescent/solar line flux is highly uncertain.

4. The measured ~1.01 MeV line energies in both spectra are consistent with an origin from ^{10}B (1.022 MeV) produced in (n, $n\alpha$) and (p, $p\alpha$) reactions on ^{14}N. The solar-event line has a width that is ≤ 4%, while there is evidence that the width of the quiescent feature is broader. If this line comes from deexcitation of the 1.740 MeV level to the 0.718 MeV level in ^{10}B, then we would expect the flux in the 0.718 MeV line to be higher than that of the 1.022 MeV line. The ~0.72 MeV flux is ~6 times the flux in the ~1.01 MeV feature in the solar-event spectrum, but most of this probably comes from ^{14}N. The fluxes of the ~0.72 and ~1.01 MeV features are roughly comparable in the cosmic ray spectrum, with large uncertainties. The broader width of the quiescent 1.01 MeV feature suggests that other lines also contribute. The high quiescent/solar flux ratio also suggests that there are additional lines that contribute to the feature in the cosmic ray spectrum. The fact that HEAO 3 did not detect the

feature line is additional evidence that several lines contribute.

5. The primary contribution to the ~1.63 MeV feature comes from emission of a 1.635 MeV gamma ray in the deexcitation of the 3.948 MeV level to the first-excited state at 2.312 MeV in ^{14}N. The line was well observed in both the quiescent and solar-event spectra and by the HEAO 3 spectrometer (see section 4.1). As expected from the decay scheme, the flux in the 1.635 MeV line is about half that observed in the 2.313 MeV line. A small contribution may come from ^{15}O (1.618 MeV) produced in (*n*, *2n*) or (*p*, *t*) reactions on ^{16}O; there is no evidence for this line in the HEAO 3 spectrum, however.

6. The solar-event spectrum reveals a resolved line near 1.995 MeV having a width of ~3%. The energy is close to the first-excited state in ^{11}C (2.000 MeV) that is produced in (*p*, α) reactions on ^{14}N. The flux in the line is ~20% that observed in the 2.313 MeV line. This is too weak to have been detected in the quiescent atmospheric spectrum either by SMM or HEAO 3. The 1.997 MeV line comes from the 9.154 MeV level in ^{15}N that should also produce stronger lines at 5.270 and 6.322 MeV. A feature near 6.332 MeV is ~4 times more intense than the line near 1.995 MeV but has a width of 9.3% FWHM and is likely to be made up of more than one line.

7. A moderately broadened (~5% FWHM) line feature at ~2.14 MeV is evident in the quiescent spectrum that is not visible in the solar-event spectrum. We believe that the feature in the quiescent spectrum is dominated by the first-excited state of ^{11}B (2.124 MeV) that is produced in (*n*, α) reactions on ^{14}N. If it had been from ^{10}B (2.154 MeV), we would have expected the flux from the first-excited state at 0.718 MeV to be even stronger. In fact the flux in the ~0.74 MeV feature, which is probably dominated by ^{14}N, is in fact no more the 50% of the flux in the 2.14 MeV feature. The HEAO 3 spectrometer also detected the 2.124 MeV line with a statistical confidence of over 4 σ. This identification of the source of this line has implications for the strong line observed at ~4.44 MeV (width of ~3.5 %) because the second-excited state of ^{11}B produces a line at 4.444 MeV (see discussion below in paragraph 15). The lack of a resolved ^{11}B line in the solar-event spectrum is probably due to the lower cross section for the (*p*, *2pd*) reaction. We also note that we did not find an ^{16}O line at 2.190 MeV in the nuclear tables that was listed by *Letaw et al.* [1989]

8. The feature at 2.31 MeV is discussed in detail above and is produced in the transition from the first-excited state to the ground state in ^{14}N (2.313 MeV). The width of the solar-event line is well measured and is consistent with what was measured by HEAO 3 for its counterpart in the quiescent spectrum (see section 4.1). There are weak contributions from ^{11}B, ^{13}N, and ^{15}N expected in this region.

9. Both spectra reveal the presence of a feature near ~2.8 MeV. The feature from the solar event has a well-defined energy of ~2.79 MeV and a width of ~4.5%. It is most likely due to deexcitation of the 5.106 MeV level to the 2.313 MeV first-excited state in ^{14}N. The 2.793 MeV/5.106 MeV intensity ratio is expected to be 0.24 based on their branching ratios. Our measurement for the solar event indicates a ratio of 0.6 ± 0.1. *Willett and Mahoney* [1992] found a ratio of 0.35 ± 0.20 for the quiescent spectrum using HEAO 3. This suggests that lines from ^{16}O (2.741 MeV) and ^{10}B (2.868 MeV) may also contribute.

10. Both SMM spectra reveal line features near ~3.1 MeV possibly from the first-excited state of ^{13}C (3.089 MeV) and deexcitation from the 8.907 MeV level to the 5.834 MeV level of ^{14}N (3.073 MeV). The measured width is 5–10%, suggesting that other weak lines also contribute. The quiescent/solar flux ratio is uncertain but suggests more efficient production of this feature from the harder cosmic ray spectrum.

11. Both spectra reveal the presence of an ~3.38 MeV line with energies consistent with deexcitation of the 5.691 MeV level of ^{14}N to its first-excited state with the emission of a 3.378 MeV gamma ray. The width of the line produced in the solar event is 3.1 ± 1.1%; consistent with the 2% widths found for the 1.63 and 2.31 MeV lines. The flux in the 3.38 MeV line from the solar event is ~20% of that observed in the 2.313 MeV line. In contrast the feature in the quiescent spectrum is broader, and its flux, although uncertain, appears to be comparable with the flux in the 2.313 MeV line. This suggests that other lines may contribute to this line feature, possibly from high-excited states of ^{14}N and ^{16}O: the 3.384 MeV gamma ray from the 8.490 MeV level in ^{14}N and the 3.439 MeV gamma ray from the 10.957 MeV level in ^{16}O. The high quiescent/solar-event flux ratio also suggests additional contributions to the feature in the quiescent spectrum. The excited state that produces the 3.378 MeV line should also produce a line at 5.690 at ~50% of the flux. J. R. Letaw (unpublished report, 1988) suggested the presence of such a line but we were unable to separate it from the first escape peak of the line feature at 6.13 MeV.

12. Both SMM spectra reveal line features near ~3.7 MeV expected from the second-excited state of ^{13}C (3.684 MeV). The line is broadened by between 5 and 10% owing to its spallation origin and the presence of a nearby line at 3.674 MeV from the 9.509 MeV level in ^{14}N. The quiescent/solar flux ratio is uncertain but suggests more efficient production of this line from the harder cosmic ray spectrum.

13. The ~3.9 MeV line is relatively well resolved from the line at ~3.7 MeV in both the quiescent and solar-event spectra. It may be due to emission of a 3.890 MeV gamma ray in deexcitation from the 6.204 to 2.313 MeV levels in ^{14}N. The width of the line is not well determined in either spectrum but does not exceed ~6%. The flux in the 3.89 MeV line from the solar event is ~20% of that observed in the 2.313 MeV line. In contrast the line flux in the quiescent spectrum, although uncertain, appears to be comparable with the flux in the 2.313 MeV line. This suggests that other lines contribute to the feature such as those from the third-excited state of ^{13}C (3.853 MeV) and from the 10.957 MeV excited state of ^{16}O (3.839 MeV).

14. The ~4.1 MeV line lies relatively close to more intense features at both lower and higher energies that affect the determination of its width and flux. A nearby line is expected at 4.179 MeV from deexcitation of the 11.096 MeV state of ^{16}O, but the measured width is larger than one would expect from a single deexcitation state based on what we have observed from ^{14}N, however. This line is only 20% as strong as the 2.313 MeV line from the first-excited state of ^{14}N in the solar event as might be expected; however, it is comparable in intensity to that line in the quiescent spectrum. This once again suggests that other lines contribute to this feature, especially in the quiescent spectrum.

15. The ~4.4 MeV line is the strongest resolved feature observed in both spectra aside from the annihilation line. *Ling* [1975] attributes the feature in the quiescent

atmospheric spectrum primarily to deexcitation of the second-excited state of ^{11}B. *Letaw et al.* [1989] suggested that the 4.438 MeV line from ^{12}C could contribute up to 30% of the flux. The measured widths in both spectra are close to each other and that observed by HEAO 3 and represent a Doppler broadening of 3–4%. This is larger than what is found for the ^{14}N deexcitation lines. The high quiescent/solar event flux ratio reflects the harder spectrum of cosmic radiation that produces more reaction products. Detection of the line in the quiescent spectrum at 2.124 MeV from the first-excited state of ^{11}B may help to determine the contribution of ^{12}C to the 4.4 MeV feature. The flux in the 2.124 MeV line (first-excited state) measured by both SMM and HEAO is only ~15% of the flux in the 4.444 MeV line (second-excited state). This suggests ^{11}B contributes less than 20% of the flux measured in the quiescent 4.44 MeV feature. In addition to the ^{12}C line, we find a nearby line at 4.402 MeV from the 9.509 MeV excited state of ^{14}N. Production of ^{12}C via (*p*, *pd*) is favored even more over ^{11}B (*p*, 2*pd*) in the solar-event spectrum and explains why the 2.124 MeV line is not clearly detected in that spectrum.

16. The weak ~4.8 MeV feature is found in both spectra below the stronger ~5.1 MeV line. The energy and width of the feature during the solar event are somewhat better determined. The feature lies near the 4.803 MeV line from ^{11}C. We would expect that the 4.914 MeV line from the third-excited state of ^{14}N to also contribute, although it is outside the estimated uncertainty in energy.

17. The ~5.1 MeV feature is clearly observed in both spectra, and the center energies agree, however, there is some disagreement in the width. The 5.105 MeV line from deexcitation of the fourth-excited state of ^{14}N is a likely source of the feature. This line comes from the same 5.106 MeV state that is reached during emission of the 0.728 MeV line from the 5.834 MeV state. The fact that the intensity of the 5.105 MeV line is about twice that of the 0.718 MeV line is consistent with this origin. The quiescent/solar flux ratio is 2.2 ± 0.6; this suggests additional contributions from the first-excited state of ^{15}O (5.182 MeV) and from the 11.096 MeV level in ^{16}O (4.966 MeV), especially for the quiescent spectrum. The width of the solar-event line is ~3%, while that in the quiescent spectrum is ~6%. The broader width of the line feature in the quiescent spectrum is also consistent with the presence of additional lines.

18. The ~5.8 MeV feature is weak and is only detectable in the solar-event spectrum. It is difficult to separate it from the first escape and Compton edge of the 6.1 MeV line. The large error in the intensity is due to the uncertainty in line width. It is most likely from deexcitation of the 5.834 MeV level in ^{14}N to the ground level. This transition has a branching ratio of 20% relative to the transition that produces the 0.728 MeV line. The relative fluxes observed in 0.72 and 5.8 MeV features are consistent with this ratio. We list the 5.581 MeV line from ^{11}B for completeness.

19. This ~6.1 MeV line is clearly resolved in both the quiescent and solar-event spectra and its energies and widths are in agreement. The Doppler broadening is 1–2%, consistent with what is found for the 1.6 and 2.3 MeV lines from ^{14}N. The best-fit energies appear to be higher than the energy for the deexcitation line at 6.129 MeV from ^{16}O. In addition the line profile in the solar event appears to have a shoulder near 6.2 MeV when viewed at higher resolution than presented in Figure 3. In contrast, the HEAO energy measurement is consistent with 6.129 MeV, although the line profile may also exhibit evidence two lines in close proximity. The apparent shift to high energies in the SMM data could be due to contributions from the spallation product ^{15}O at 6.175 MeV and from ^{14}N at 6.202 MeV. From the branching ratios for the 6.204 MeV level in ^{14}N, we would expect the 3.890 MeV line to be a factor of 3 higher than the 6.202 line. This suggests that the ^{14}N line accounts for no more than 20% of the flux in the 6.1 MeV line in the solar-event spectrum. Its contribution in the quiescent spectrum can be greater. The quiescent/solar flux ratio of 2.1 ± 0.5 is also suggestive of other line contributions.

20. The broad ~6.3 MeV feature is more identifiable in the solar-event spectrum. There are several lines, a few of which are listed in Table 2, which can contribute to the feature. The quiescent/solar event flux ratio is also indicative of additional lines in the cosmic ray generated spectrum.

21. Deexcitation lines from both ^{14}N (7.027 MeV) and ^{16}O (6.917 and 7.117 MeV) can contribute to the relatively broad ~7.0 MeV line feature, as well as a line from ^{14}C. The features in both spectra are broadened ~4% for the solar event and ~6% for the quiescent spectrum suggesting contributions from more than one line. The fluxes in the 6.9 MeV line features are also ~2 and ~3 times higher than the flux in the ~6.1 MeV line. This is consistent with fluxes coming from two or three lines each with a flux comparable to the 6.1 MeV line.

5.4. Origin of the Unresolved Nuclear Continuum

We have revealed remarkable residual components in Figures 2b and 3b after subtraction of the resolved nuclear lines, listed in Tables 1 and 2, and electron bremsstrahlung continua from the quiescent and solar-event spectra. We initially discovered these components when we found that very broad Gaussians were required to fit the atmospheric spectra. The shapes of these residuals differ from what we calculate would be produced by Compton scattering of the individually resolved atmospheric lines in a few gm/cm^2 of nitrogen. The dashed lines in Figures 2b and 3b represent the spectra of photons after scattering (the normalization is arbitrary). We note some important differences between the residual components in the quiescent and solar-event spectra. It is surprising to find that the residual flux in the quiescent spectrum is ~10% more intense than the summed contribution from all the resolved lines; this can be seen by comparing the sum of resolved lines in Figure 2a with the residual spectrum in Figure 2b. In contrast, the residual flux in the solar-event spectrum (Figure 3b) is only ~30% as intense of the sum of resolved lines (Figure 3a). There are also some differences in the shape. The broad feature near 5 MeV accounts for about 2/3 of the residual component in the solar-event spectrum but only ~1/3 of the residual in the quiescent spectrum. What is the source of these residual features?

To help answer this question we replot the residual quiescent and solar-event spectra in Figures 6a and b, respectively. The shape of these residuals is unlike any that we might expect from a continuum related to radiation from electrons. It appears to reflect what one might expect to observe from several lines that are not individually resolved in the NaI detectors. The fact that the residual is much stronger in the quiescent spectrum suggests to us that it is likely to be produced by atmospheric neutrons. This leads us to consider the effects of thermal neutron capture. As

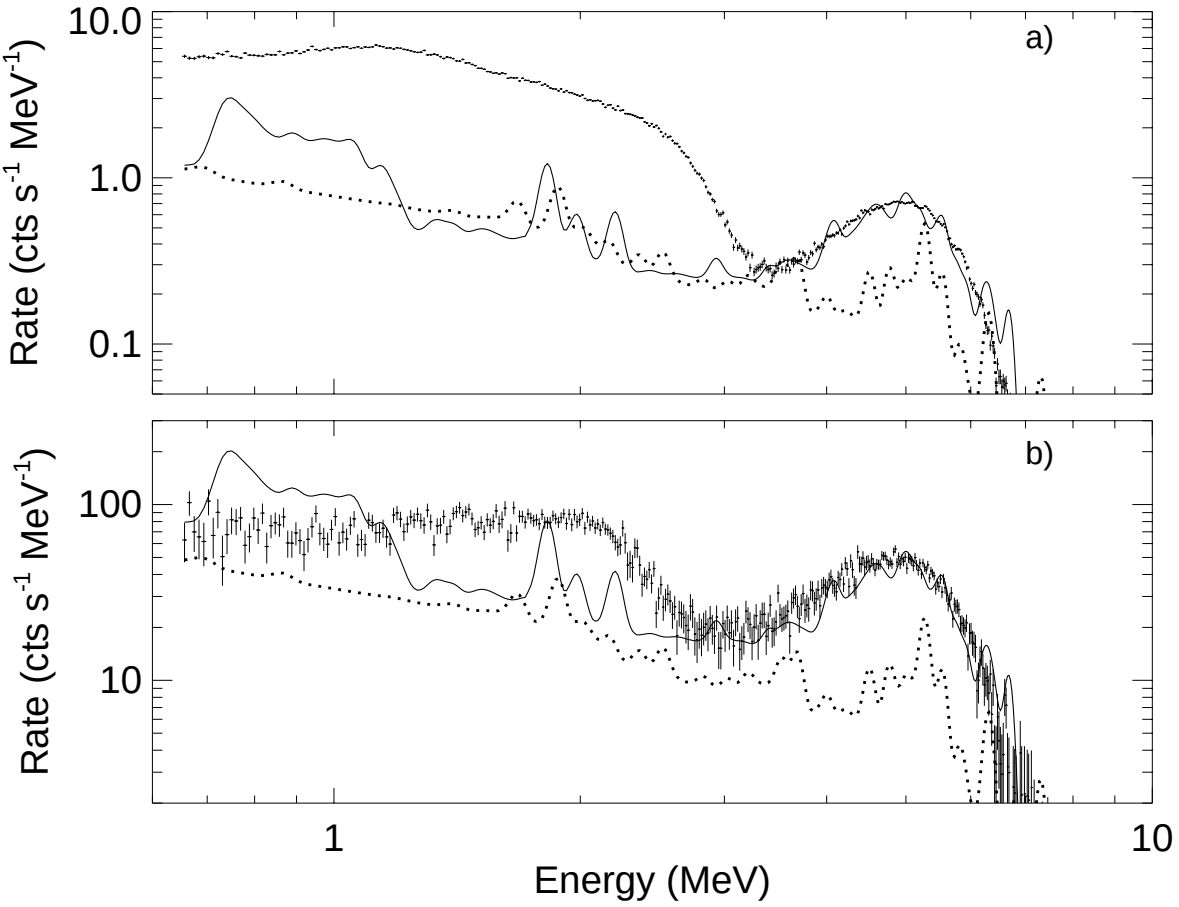

Figure 6. The residual spectrum after subtraction of the 20 resolved nuclear lines and power law continuum. Solid curve shows expected response (arbitrary normalization) to multiple gamma ray lines emitted from iodine (in the NaI detector) after thermal neutron capture. Dotted curve is the response (arbitrary normalization) from neutron capture on atmospheric nitrogen. (a) Quiescent spectrum from cosmic ray interactions. (b) Spectrum from interaction of solar energetic particles.

heavy nuclei have a larger number of excited states, lines from capture on such elements are more likely to be blended. For this reason we have calculated the response of the instrument to neutron capture on iodine in the NaI detectors. We folded the prompt capture gamma ray lines listed by *Lone et al.* [1981] through the SMM instrument response. We plot the results of this calculation as solid lines in Figure 6; the normalization is arbitrary. The overall shape of the calculated response is in remarkably good agreement with the broad feature near 5 MeV in the residual spectra near 5 MeV, providing compelling evidence for an association with neutron capture. The observed spectra deviate from the calculations at lower energies. There are several other elements in the satellite and the Earth's atmosphere which contribute capture lines that are likely to account for the remainder of the residual spectra. As an example, we also plot the instrument's response to capture lines from atmospheric nitrogen at a depth of ~20 gm cm^{-2}. A complete analysis of the effects of neutron-capture will require considerably more work and is beyond the scope of this paper.

6. Summary and Conclusions

We have compared spectra of gamma ray lines and continua produced in the Earth's atmosphere by cosmic ray irradiation and by proton bombardment from an intense solar-energetic particle event. Our study of the quiescent spectrum from cosmic ray impact, accumulated over a 9-year period, is an incremental improvement over a detailed study performed by *Letaw et al.* [1989] on a more limited set of data. We list the energies and widths of 20 resolved gamma ray lines observed and identify nuclei that may be responsible for the emission. The observations have been performed with a moderate resolution spectrometer on NASA's SMM satellite that typically monitored the atmosphere at magnetic rigidities > 2 GV. The gamma ray lines are primarily produced by interactions of neutrons ejected when the high-energy cosmic ray particles break up atmospheric nitrogen and oxygen. Many of the lines come from direct excitation of atmospheric ^{14}N and ^{16}O; an equivalent number are emitted from isotopes produced by spallations of these nuclei by the neutrons or cosmic rays.

These neutrons thermalize and are likely to be the origin of a newly discovered unresolved nuclear component in the detector that is produced by neutron capture.

The solar energetic particle event occurred on October 20, 1989, when a shock from an intense flare and coronal mass ejection reached Earth. Protons down to MeV energies from this event interacted with the atmosphere visible on the southern horizon from SMM. The overall atmospheric gamma ray flux increased by a factor of ~40 over its quiescent value. The increase in total resolved nuclear line flux was about 4 times the increase in electron bremsstrahlung flux. This occurs because the softer spectrum of solar energetic particles is less efficient than the cosmic rays in producing electromagnetic showers. The latter is reflected in the increased atmospheric depth where electron-positron annihilation occurs. We list the energies and widths of the 20 resolved nuclear lines and identify their origins.

We also have evidence that the spectrum of cosmic ray produced neutrons is harder than the spectrum of shock-produced protons. This is based on the larger number of gamma rays observed in the quiescent spectrum from nuclei produced by high-energy nuclear reactions and spallation. More directly we can use the ratio of two nuclear lines to estimate the spectrum of interacting protons in the shock event. Calculations of line yields have been performed using a computer code [*Ramaty et al.*, 1979]. This technique has been successfully applied to determination of the spectra of flare-accelerated protons and α-particles at the Sun [*Ramaty et al.*, 1995]. We choose two resolved lines that are sensitive to particles of different energy: the 1.635 MeV ^{14}N line produced by direct excitation and the 4.44 MeV ^{12}C line produced by the (p, t) reaction on ^{14}N. The line ratios for various power law indices have been calculated using the gamma ray production code cited above. Because it is optimized for solar flares it currently does not include production of the nearby ^{11}B line; however, we have shown in section 5.3. that the line from ^{12}C is likely to dominate. Assuming a power-law proton spectrum for the solar particle event, we obtain a differential index of about −3.3. If the contribution from ^{11}B had been included, the spectrum would have been even steeper. The estimated spectrum appears to be steeper than the one measured using the GOES proton detector in geosynchronous orbit during the particle event. More detailed analysis is required to determine whether these spectral differences are real and whether propagation into the magnetosphere plays a role.

From this cursory discussion it is clear that significant new information about the spectra of protons that reach the Earth during solar particle events can be obtained from atmospheric gamma ray observations. This provides information on the transport of particles through the magnetosphere during geomagnetically disturbed periods if comparisons can be made with particle measurements outside the magnetosphere. Future gamma ray instruments can remotely monitor and image the impact of solar-energetic particles on the atmosphere. This will complement direct observations of protons transmitted through the magnetosphere when they are available, such those made by the NOAA 10 satellite [*Boberg et al.*, 1995].

What is required is an extension of the gamma ray production code to include additional cross sections for reactions relevant to the Earth's atmosphere. A further extension of the code to include neutron excitation and reaction cross sections of ^{14}N and ^{16}O will enable us to determine the spectra of cosmic ray produced neutrons in the atmosphere using remote observations with gamma ray spectrometers. The excellent observations made by the HEAO 3 germanium spectrometer demonstrate the value of high-resolution gamma ray line observations of the atmosphere. We anticipate that NASA's High Energy Solar Spectroscopic Imager (HESSI) planned for launch in 2001 will provide improved gamma ray spectra.

Acknowledgments. This work was partially supported by NASA under DPR W-18,995 and by the Office of Naval Research. We wish to acknowledge Erich Rieger for his discovery of the solar particle event in the SMM data and his early analysis of this event with Jim Ryan. We also thank Alan Tylka for discussions concerning the solar particles and their transport to Earth. James Kurfess suggested that we investigate whether thermal neutron capture could explain the unresolved continuum that we observe in the atmospheric spectra. We are indebted to Reuven Ramaty for allowing us to use his gamma ray production code to estimate the proton spectrum reaching the atmosphere in the solar energetic particle event.

Janet G. Luhman thanks the referees for their assistance in evaluating this paper.

References

Boberg, P. R., A. J. Tylka, and J. H. Adams, Jr., Geomagnetic transmission of solar energetic protons during the geomagnetic disturbances of October 1989, *Geophys. Res. Let., 22,*1133-1136, 1995.

Coffey, H. E. (Ed.), *Solar-Geophysical Data, 543, Part I,* p.13, Nat'l Geophys. Data Cntr, Boulder, 1989.

Firestone, R. B. and V. S. Shirley (Eds.), *Table of Isotopes Eighth Addition*, John Wiley, New York, 1996.

Forrest, D. J. *et al.*, The gamma ray spectrometer for the Solar Maximum Mission*, Solar Phys., 65*, 15-23, 1980.

Lampton, M., B. Margon, and S. Bowyer, Parameter estimation in x-ray astronomy, *Astrophys. J.*, *208*, 177-190, 1976.

Letaw, J. R., G. H. Share, R. L. Kinzer, R. Silberberg, E. L. Chupp, D. J. Forrest, and E. Rieger, Satellite observation of atmospheric nuclear gamma radiation, *J. Geophys. Res*., *94*, 1211-1221, 1989.

Ling, J. C., A semiempirical model for atmospheric gamma rays from 0.3 to 10 MeV at 40°, *J. Geophys. Res., 80*, 3241-3252, 1975.

Lockwood, J. A., L. Hsieh, L. Friling, C. Chen, and D. Swartz, Atmospheric neutron and gamma ray fluxes and energy spectra, *J. Geophys. Res*., *84*, 1402-1408, 1979.

Lone, M.A., R. A. Leavitt, and D. A. Harrison, Prompt gamma rays from thermal-neutron capture*, At. Data and Nucl. Data Tables*, *26*, 511-559, 1981.

Mahoney, W. A., J. C. Ling, and A. S. Jacobson, HEAO 3 measurements of the atmospheric positron annihilation line, *J. Geophys. Res*., *86*, 11,098-11,104, 1981.

Murphy, R. J., Gamma rays and neutrons from solar flares, Ph.D. dissertation, Univ. of Md., College Park, 1985.

Murphy, R. J., G. H. Share, J. R. Letaw, and D. J. Forrest, Nuclear line spectroscopy of the 1981 April 27 solar flare, *Astrophys. J., 358*, 298-312, 1990.

Ramaty, R., R. B. Kozlovsky, and R. E. Lingenfelter, Nuclear gamma rays from energetic particle interactions, *Astrophys .J. Suppl., 40*, 487-526, 1979.

Ramaty, R., N. Mandzhavidze, B. Kozlovsky, and R. J. Murphy, Solar atmospheric abundances and energy content in flare-accelerated ions from gamma ray spectroscopy, *Astrophys. J. Lett., 455*, L93-L96, 1995.

Ryan, J. M., A. C. Aikin, E. W. Cliver, E. Rieger, and G. H. Share, Solar-terrestrial science, in *The Many Faces of the Sun,* edited by K. T. Strong *et al.*, Springer-Verlag, New York, pp. 457-479,

1999.
Share, G. H., R. L. Kinzer, J. D. Kurfess, D. C. Messina, W. R. Purcell, E. L. Chupp, D. J. Forrest, and C. Reppin, SMM detection of diffuse galactic 511 keV annihilation radiation, *Astrophys. J., 326*, 717-732, 1988.
Share, G. H., R. L. Kinzer, M. S. Strickman, J. R. Letaw, E. L. Chupp, D. J. Forrest, and E. Rieger, Instrumental and atmospheric background lines observed by the SMM gamma ray spectrometer, in *High-Energy Radiation Background in Space, AIP Conf. Proceedings, 186*, edited by A. C. Rester, Jr., and J. I. Trombka, pp. 266-277, AIP, New York, 1989.
Share, G. H., R. J. Murphy, and E. Rieger, Atmospheric gamma ray lines produced by cosmic rays and solar energetic particles, *26th Int. Cosmic Ray Conf.*, *7,* 329-332, 1999.
Tylka, A. J., J. H. Adams, P. R. Boberg, B. Brownstein, W. F. Dietrich, E. O. Flueckiger, E. L. Petersen, M. A. Shea, D. F. Smart, and E. C. Smith, CREME96: a revision of the cosmic ray effects on micro-electronics code*, IEEE Trans. Nucl. Sci., 44* (6), 2150-2160, 1997.
Willett, J. B., and W. A. Mahoney, High spectral resolution measurement of gamma ray lines from the earth's atmosphere, *J. Geophys. Res., 97*, 131-139, 1992.

R. J. Murphy, and G. H. Share, E. O. Hulburt Center for Space Research, Code 7652, Naval Research Laboratory, 4555 Overlook Ave., Washington, D.C., 20375. (murphy@gamma.nrl.navy.mil; share@gamma.nrl.navy.mil)

(Received February 24, 2000; revised June 9,2000; accepted June 9, 2000.)